Tribology International 180 (2023) 108240

Contents lists available at ScienceDirect

Tribology International

journal homepage: www.elsevier.com/locate/triboint

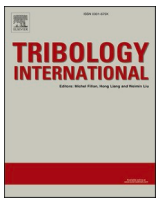

The static friction peak in reciprocating sliding

Saad Bin Jaber [a,b], Yang Xu [c,*], Mehmet E. Kartal [d], Nikolaj Gadegaard [a], Daniel M. Mulvihill [a,*]

[a] James Watt School of Engineering, University of Glasgow, Glasgow G12 8QQ, UK
[b] Department of Physics, College of Sciences, Al-Imam Mohammad Ibn Saud Islamic University (IMSIU), Riyadh 11623, Saudi Arabia
[c] School of Mechanical Engineering, Hefei University of Technology, Hefei, China
[d] School of Engineering, University of Aberdeen, Aberdeen AB24 3UE, UK

ARTICLE INFO

Keywords:
Static friction peak
Reciprocating sliding
Gross-slip fretting
Frictional hysteresis loop

ABSTRACT

This paper investigates why the static friction peak is mostly absent in reciprocating sliding and gross-slip fretting literature. Here, reciprocating sliding tests were conducted on ultra-smooth silicon surfaces. A prominent static friction peak was present in the initial cycles. However, a rapid wear-induced decay in the static friction peak occurred after the first cycle with the peak being mostly absent by about 30 cycles. Two possible explanations are proposed for the wear-induced decay: (1) that increasing surface roughness (with cycles) reduces the fully stuck contact area and (2) that wear reduces the bonding strength of the stuck interface by removing third body contaminant molecules. Predictions from a multi-asperity friction model are used to support these arguments.

1. Introduction

The static friction force F_s is the force needed to initiate sliding between surfaces and kinetic friction F_k is the force required to maintain sliding at some velocity. Very often, in experiments on friction (in unidirectional sliding), the static friction is greater than the kinetic friction and this leads to the so called static friction peak [1]. However, in reciprocating sliding and gross-slip fretting, the static friction peak is hardly ever observed in the literature. This raises interesting questions about why it is not observed and the circumstances under which the peak might be observed in reciprocating sliding. In this paper, we explore this question on the existence of the static friction peak specifically in the reciprocating sliding scenario.

Before focusing on reciprocating sliding, it is worth addressing existing theory on the static friction peak. The first thing to note is that the magnitude of static friction is generally accepted to be dependent on the time of (static) contact for many materials including metals and polymers [2–7]: this is known as frictional ageing [5]. Contacts left static for longer times require a bigger force to initiate sliding. This is often explained via a time dependent growth of the real contact area via processes such as thermally activated creep [2,8]. In general, we can think of either static or kinetic friction F as arising from shear resistance at the real areas of contact so that $F = \tau A_r$ [9], where τ indicates an effective shear strength of the interface and A_r is the real contact area. However, the transition from static contact to full sliding is subtle and assumptions about contact area have often been difficult to verify as the contact is frequently unobservable. However, recent advances in in-situ high resolution measurement of contact area have been able to shed more light on this. For example, Weber et al. [10] made accurate high resolution measurements of contact area during the three key stages of contact for a polystyrene (PS) sphere in contact with glass coated with pressure sensitive rigidochromic molecules: (1) ageing of the fully stuck contact, (2) the transition from stick-to-slip (pre-sliding) and (3) full sliding. In their experiments, they observed the contact area growth during ageing of the 'fully stuck' contact, but noted that this produced an increase in the kinetic friction level as well as the static friction level (although, the gap between the two ΔF - the static friction peak - did increase slightly with the fully-stuck ageing time). One could easily ask whether another possibility for the lower level of kinetic friction (as compared to static) might be the so called shear induced contact area reduction that occurs in pre-sliding (mostly in softer materials like polymers) under the application of tangential force [10,11] (i.e. the idea being that A_r might be lower during sliding). However, the Weber et al. [10] experiments found that the majority of shear induced contact area reduction had already occurred by the time the maximum friction peak was reached. In fact, real contact area A_r then increased very slightly ($\sim$ 1%) during sliding. This led the authors to conclude (according to $F = \tau A_r$) that the interface must have weakened (i.e. effective τ must have reduced) to explain the friction drop from static peak to steady state kinetic. Therefore, another plausible reason for the friction drop from

* Corresponding authors.
E-mail addresses: Yang.Xu@hfut.edu.cn (Y. Xu), Daniel.Mulvihill@glasgow.ac.uk (D.M. Mulvihill).

https://doi.org/10.1016/j.triboint.2023.108240
Received 29 June 2022; Received in revised form 16 December 2022; Accepted 7 January 2023
Available online 9 January 2023

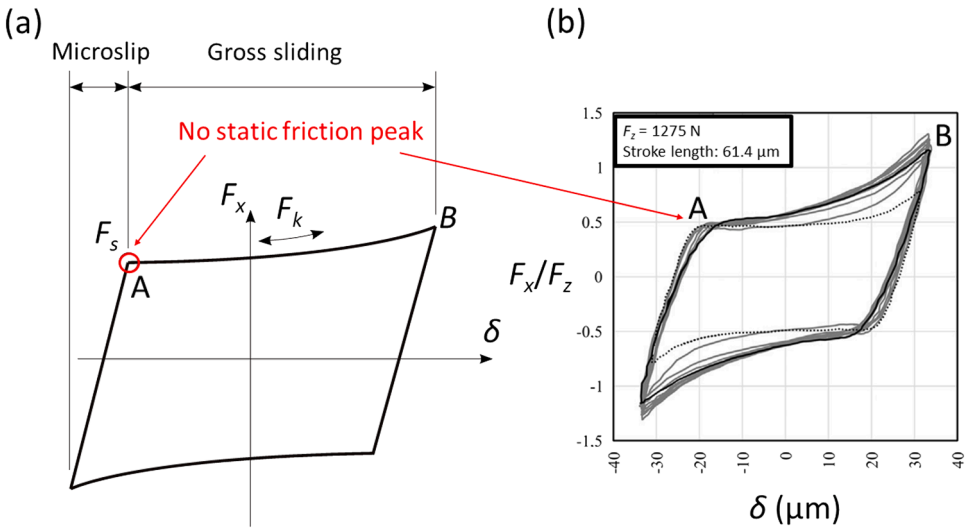

Fig. 1. (a) Schematic illustration of a typical frictional hysteresis loop in reciprocating sliding and (b) experimentally measured loops from aluminium bronze in contact with steel from Hintikka et al. [32] (ranging from the dotted loop at 5000 cycles to the black loop at 100 $\times 10^3$ cycles with the grey loops in between being taken at 10,000 cycle spacing). Note the absence of any static friction peak – this is typical of the vast majority of reciprocating sliding and gross slip fretting results.

static to sliding might be an accompanying reduction in the shear strength of the interface. The origin of this shear strength is generally accepted to arise from chemical bonding interactions (at least for stuck contacts and for low velocity sliding) [9,11–13]. Indeed, Filippov et al. [13] notes that the probability of bond formation depends on the time of contact so the lower time available for bonding during sliding may explain some of the differences between the strength of static and sliding contacts. According to Budakian and Putterman [12], the chemical bond formation and rupture argument is also sufficient to explain the commonly observed stick-slip phenomenon. Li et al. [7] provided evidence that frictional ageing can also result from chemical bond development. They argued that, at the nanometer scale, at relatively low contact pressures and for hard brittle materials, frictional ageing cannot be explained by increases in contact area due to plastic creep. At the nanometer scale, using silica AFM tips in contact with silica, they found slow logarithmic ageing resulting in an increase in static friction with time of contact and showed that this was due to strengthening of chemical bonding rather than contact area growth. The magnitude of the static friction peak (or friction drop) ΔF grew linearly with the logarithm of hold/ageing time. However, the effect was far more pronounced than for equivalent macroscopic rough contacts. The relative static friction peak (or relative friction drop) $\Delta F/F_k$ for the nanoscale AFM contact ranged from 0.5 to 5 for a 100 s hold time, while the equivalent relative peak value for the macroscale contacts was less than 0.05. The implications of the Li et al. experiments for macroscale rough contacts are not fully resolved, but Li et al. surmised that the smaller frictional ageing effect in macroscale contacts is likely due to the asperities in the macroscale contact all being at different stages in their evolution from stick to slip. Li et al. also used two surfaces that would not be expected to form bonds (hydrogen terminated diamond and graphite) and found no difference between static and kinetic friction. Therefore, in $F = \tau A_r$, it is likely that both τ and A_r can be altered by parameters such as time of contact and tangential force. Xu et al. [14] developed a contact mechanics based model of the transition from static to sliding friction for the rough surface scenario. By implementing a fracture mechanics approach at each contacting asperity [15] that considers pre-sliding transition from stick to full sliding as the propagation of an interfacial crack through the bonded interface (at each asperity contact) under mixed mode loading, the model was able to reproduce a static friction peak primarily arising from the fracture toughness of the fully stuck bonded asperity contacts (i.e. interfaces with higher work of adhesion (or smaller mode mixity) gave a more pronounced static friction peak). The implementation in Xu et al. [14] of the asperity level model to the rough surface case was handled via a Greenwood and Williamson [16] approach to the surface statistics. Interestingly, friction studies carried out by Vlassov et al. [17] on ZnO nanowires inside an SEM also suggest that the overcoming of static friction is governed by reaching unstable propagation of a crack through the interface. As noted by Weber et al. [10], the detailed mechanism behind the static friction peak may not be universal and may depend on the specific material pair and the surrounding environment. For instance, He et al. [18] noted that any surface exposed to air will likely adsorb small hydrocarbon molecules and they proposed a theory of static friction based on third body layers of molecules that act to lock the surfaces together. In the case of humid environments, Persson et al. [2] mentioned the formation of capillary bridges and in the case of polymer contacts, they cite the mechanism of chain interdiffusion of polymers in static contacts. In well-bonded clean metal contacts (such as for outgassed virgin metal surfaces in vacuo), shear induced junction growth (of the real contact area) can occur during pre-sliding leading to very large contact area and static friction levels [19–22] (i.e. the opposite of the shear induced contact area reduction in softer materials). It is clear therefore that the mechanism producing the static friction peak is somewhat dependant on the circumstances (materials, surface layers, temperature and environment). However, like most friction phenomenon, the static friction peak behaviour is likely governed by some combination of real contact area and chemical bonding interactions.

We return now to the issue of static and kinetic friction in reciprocating sliding. Reciprocating sliding is the case were repeated cycles of nominally identical sliding occur with the sliding direction being rapidly reversed at the end of each stroke. Frictional behaviour in reciprocating sliding is generally characterised by measuring frictional hysteresis loops (plots of tangential force F_x versus displacement δ – see Fig. 1a). Reciprocating sliding tests are an important way of assessing the wear performance of materials. They can be used to assess the durability of coatings and surface treatments etc. The energy dissipated is the area enclosed in the loop and this energy is then lost in heat generation and acoustic emission as well as in the plastic deformation and fracture processes that produce wear debris. Reciprocating sliding where the stroke length is a small fraction of the contact patch (often tens or hundreds of microns) is commonly referred to as gross-slip fretting – a situation which often occurs in contacts and joints in vibrating machinery. To the best of the author's knowledge, a static friction peak is rarely ever observed in experimental reciprocating sliding or gross-slip

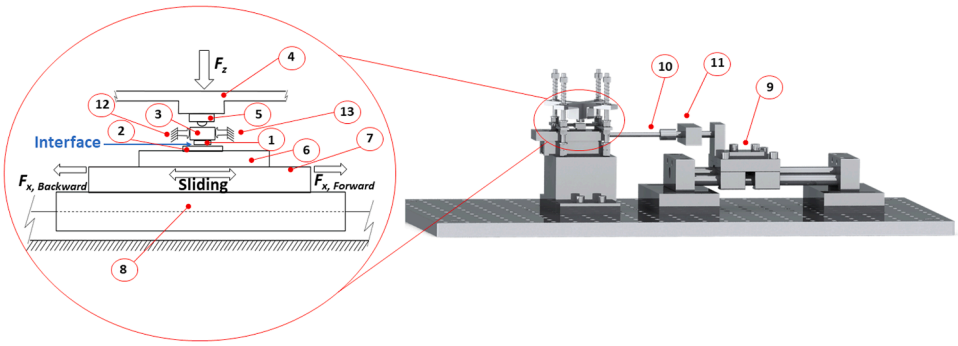

Fig. 2. Schematic representation of the reciprocating sliding rig: (1) upper silicon specimen, (2) lower silicon specimen, (3) upper backing block, (4) upper arm, (5) button load cell, (6) lower backing block, (7) low fiction bearing, (8) base plate, (9) linear stage, (10) Connecting rod, (11) Tension/compression load cell and (12 and 13) motion limiting stoppers (Note: the motor is not shown here).

fretting tests in the literature [23–34]. Fig. 1b shows a typical test result from the literature [32]. This result is from tests on aluminium bronze against steel at various cycle numbers, but is representative of results across the literature. One can see that, at the points marked A, gross sliding occurs, but without any distinguishable static friction peak. In gross slip fretting tests, a peak is often observed at the end of the sliding stroke (points marked B in Fig. 1). This is not to be confused with the static friction peak. It has been shown to be caused by wear scar interaction and has been addressed in papers by Mulvihill et al. [23] and Hintikka et al. [32,33,35]. At this point, a number of interesting questions arise: why do we not see a static friction peak in these tests and under what conditions might we be able to observe one? There is also the interesting notion that reciprocating sliding tests might be able to shed some light on the mechanisms governing the static friction peak.

In a previous work [36], we observed distinct static friction peaks in the unidirectional flat-on-flat sliding of silicon (Si) against silicon (where the samples were cut from commercial silicon wafers with nanoscale RMS roughness of about 1 nm). In the present paper, we subject the flat silicon contacts to reciprocating sliding and investigate the behaviour of any static friction peak. To help interpret the results, we implement the Xu et al. adhesive multi-asperity friction model [14] for the sliding silicon surfaces in the experiments. The model can predict an evolution for the tangential force during the transition from stick to slip and is useful to compare with experiments. The paper is arranged as follows: In Section 2, we outline the experimental aspects of the reciprocating sliding test and in Section 3 we outline the details of applying the Xu et al. adhesive friction model and the input parameters needed from the specimens. Finally, in Section 4, we outline the results and discuss their physical implications before drawing conclusions.

2. Experimental procedure

The rig used is a slightly modified version of the one developed for unidirectional sliding by the present authors in Bin Jaber et al. [36]. The approach is somewhat similar to the sled-type friction test in ASTM D1894 [37]. A schematic representation of the rig is shown in Fig. 2 (with numbers indicating the key components). The contact adopted for the study was a flat-on-flat contact with silicon sliding against silicon. The silicon samples were cut from commercial silicon wafers and therefore possess high global flatness (< 2 μm) and nanoscale RMS roughness (< 1 nm). The wafers were p-type with (100) orientation. The contact consisted of a stationary upper surface (1) pressed against a moving lower surface (2) to enable reciprocating sliding. The upper surface was cut to 10×10 mm^2 while the lower surface was longer (and wider) at 15×20 mm^2 to facilitate sufficient sliding distance and avoid edge effects (i.e. upper surface moving over one of the edges of the lower surface). The upper specimen was bonded to an upper backing block (3). Normal load F_z was transmitted to the contact by compressing four springs (via turn screws) against an upper arm (4). A 110 N button load cell (5) (LBS, Interface Force Measurements, UK) was positioned between the upper arm and the upper backing block to accurately measure the applied normal load. The button load cell has a spherical tip which allows the upper specimen to self-align with the lower specimen. The lower specimen was bonded to a lower backing block (6), which in turn, is fixed to an ultra-low friction linear bearing (7) mounted on a base plate (8). Movement of the lower specimen was achieved by a linear stage (9) connected to the lower backing block by a connecting rod (10). Tangential force F_x is measured by a 45 N universal tension/compression load cell (11) (SML, Interface Force Measurements, UK) connected in the path of the connecting rod. Actuation of the linear stage was achieved via a high torque hybrid stepper motor (NEMA 23, Lin Engineering, USA). The modification made for the present work was the introduction of stopper systems on both the left (12) and right (13) of the contact to prevent horizontal movement of the upper specimen with the lower specimen in either sliding direction (motion in only one direction was constrained in [36]). A LabVIEW program was used to control the motorised stage and record the test data. Signals from the load cells were first passed through a NI-9237 full-bridge amplifier (National Instruments, USA) before being processed by a PC. Displacement of the stage was extracted directly from the motor's control software.

Prior to testing, the silicon samples were cleaned using acetone followed by IPA and then rinsed in DI water and subsequently air blow-dried. The upper samples were then scanned in an atomic force microscope (AFM) (Bruker, USA) using ten scan areas of 10×10 μm^2 on each surface to measure surface roughness. After roughness measurement, the solvent treatment was applied again to clean the samples before the test. For the reciprocating sliding tests, a fixed normal load of 10 N was applied to the contact for the duration of the tests. Prior to sliding, the contact was held stationary under the normal load for 3 min. The contact (lower surface) was then oscillated with a stoke length of 0.5 mm for 100 cycles (total sliding per cycle of 1 mm). Steady state velocity during sliding was 0.05 mm/s. This produced a frequency of about 0.05 Hz. The test was repeated five times each time with new nominally identical samples. After testing, the samples were again scanned in the same way as before using the AFM to determine any changes in roughness.

3. Adhesive friction model for transition from stick to slip

3.1. Theoretical background

To help interpret our experimental results on the static to kinetic friction transition, we apply the multi-asperity adhesive friction model recently developed by Xu et al. [14]. This is useful because the model offers a prediction of the evolution of the tangential force, F_x, normal load, F_z, and real contact area, A_r, as an elastic nominally flat rough surface in contact with a rigid flat proceeds from fully stuck to gross sliding. The interfacial friction is induced by the coupling between the adhesion and tangential load at the contacting asperity level. This is

governed by Papangelo and Ciavarella's model which describes the transition from stick to slip based on the fracture of asperity contacts [15]. Assuming the asperity height follows the Gaussian distribution and the classical multi-asperity contact model, Xu et al. summed the tangential forces, normal loads, and real contact areas at the asperity level (i.e., T, P, πa^2 respectively) to produce predictions for a normally flat macroscale rough contact (F_x, F_z and A_r). Most interestingly, the model qualitatively predicts key phenomenon observed in friction tests, e.g., the shear-induced contact area reduction in pre-sliding (more common in soft materials) and the static friction peak. The static friction peak in the Xu et al. model essentially arises from the fracture toughness of the fully stuck contact areas at the asperity level. This is because the limiting tangential force needed to fully slide an asperity is governed by the tangential force required to fully propagate a crack through the interface which is considered to be adhesively bonded. For example (according to the model), a higher work of adhesion at the asperity contacts results in a more pronounced static friction peak.

The governing equations of the Xu et al. model [14] are:

$$F_z(d,\delta_T) = \eta A_n \int_{\delta_2}^{\infty} P_{PC}(\delta,\delta_T)\varnothing(d+\delta)d\delta + \eta A_n \int_{\delta_1}^{\delta_2} P_{Hertz}(\delta)\varnothing(d+\delta)d\delta \tag{1}$$

$$F_x(d,\delta_T) = \eta A_n \int_{\delta_2}^{\infty} T_{PC}(\delta,\delta_T)\varnothing(d+\delta)d\delta + \eta A_n \int_{\delta_1}^{\delta_2} T_{Hertz}(\delta)\varnothing(d+\delta)d\delta \tag{2}$$

$$A_r(d,\delta_T) = \eta A_n \int_{\delta_2}^{\infty} \pi a_{PC}^2(\delta,\delta_T)\varnothing(d+\delta)d\delta + \eta A_n \int_{\delta_1}^{\delta_2} \pi a_{Hertz}^2(\delta)\varnothing(d+\delta)d\delta \tag{3}$$

where η is the density of asperities, A_n is the nominal contact area (10×10 mm^2), δ is asperity normal displacement, δ_T is asperity tangential displacement and d is the separation distance between the two surfaces. For a given combination of (δ, δ_T), the contacting asperities in stick or slip stages are governed by the Papangelo and Ciavarella (PC) model and Hertzian contact theory (Hertz), respectively. The integral limits, δ_1 and δ_2, are the critical indentation depths associated with the transition between non-contact, stick and slip stages. A detailed description of the model can be found in Xu et al. [14].

3.2. Model input parameters

A key input for the Xu et al. model [14] are the parameters describing the surface topography. These parameters were extracted from AFM scans on the silicon samples acquired prior to testing and after testing. The parameters required are root mean square asperity height (σ_s), asperity density (η) and mean asperity radius (R). The extraction of these parameters from the AFM scans followed the same procedure as detailed in Xu et al. [14]. It should be noted that Xu et al. [14] used McCool's solution to numerically calculate the curvature of each asperity using central differentiation, and then the mean radius of curvature is the average of all asperity curvatures. This method was extensively discussed by Sayles and Thomas [38]. The pre-test scans represent the intact condition of the silicon surfaces before being affected by wear; whereas, the post-test scans represent the state of the roughness at the end of the test. Here, we assume that σ_s is the only variable during the test, while the other parameters remain constant. To investigate the impact of roughness changes on friction behaviour for the silicon samples, σ_s from the pre and post-test scans were assumed to be the roughness corresponding to Cycle 1 and Cycle 100, respectively. Values of σ_s for intermediate cycles were then estimated by using linear interpolation.

Mechanical properties are also required. Here, the Young's modulus E, shear strength τ and Poisson's ratio ν are sufficient. These parameters were obtained directly from Refs. [39,40] as ($E = 169$ GPa, $\tau = 10$ GPa and $\nu = 0.272$). The value of the shear strength might seem quite high, but it can be considered as a limiting value. The chosen value of the shear strength is quite accurate as the experimental results show in Section 4. An effective Young's modulus was then calculated from $E^* = E/(1\text{-}\nu^2)$.

Table 1
Total surface tension, dispersive surface tension and polar surface tension of the liquids used in the measurement of surface energy on the silicon specimen surfaces (from [42,43]).

Liquids	Surface tension - total (γ) (mN/m)	Surface tension - dispersive (γ^d) (mN/m)	Surface tension - polar (γ^p) (mN/m)
Water	72.8	21.8	51.0
Ethanol	21.4	18.8	2.6
Ethylene glycol	48	29	19

The surface energy (work of adhesion) is also a key parameter in the Xu et al. model. Here, we measured it experimentally on the pre-test silicon surfaces using the Owens, Wendt, Rabel and Kaelbel (OWRK) method [41]. This method implements contact angle measurement via dropping liquids (with known surface tensions) on the sample surface. The liquids used in the measurement were water, ethanol and ethylene glycol. To carry out the OWRK calculations, the total surface tension (γ), dispersive surface tension (γ^d) and polar surface tensions (γ^p) of the liquids are required. These were obtained from Refs. [42,43] and are presented in Table 1. Once the contact angle Θ made by droplets of the liquids impinging on the pre-test silicon surface is known, the surface energy of the silicon surface is calculated by fitting a line between the points obtained with values of Eq. (4) (below) on the abscissa (x-axis) and values of Eq. (5) as the ordinate (y-axis).

$$x\left(\gamma^p,\gamma^d\right) = \sqrt{\frac{\gamma^p}{\gamma^d}} \tag{4}$$

$$y(\Theta,\gamma^p,\gamma) = \tfrac{1}{2}(1+\cos(\Theta))\left(\frac{\gamma}{\sqrt{\gamma^d}}\right) \tag{5}$$

The slope and y-intercept components of the fitted line raised to the power 2 give the polar and dispersive components of the surface energy required (in this case, the silicon surface), respectively. The summation of these is then the required silicon free surface energy.

The contact angle between a droplet of each liquid and the pre-test silicon surface was imaged using a high resolution camera and subsequently measured in ImageJ software. Images were captured one second after the droplet touched the surface. Fig. 3 shows the shapes (and contact angles) for droplets of the same volume of each of the three liquids on the tested silicon surface. It can be seen that the water droplet occupies the smallest area (highest contact angle) on the silicon surface due to its high surface tension. On the other hand, the largest area occupied by the droplets is from ethanol, which produces the lowest contact angle as it possesses the lowest surface tension among the three liquids. The contact angle measurement was repeated three times on each of three different silicon samples. The total average surface energy of the pre-test silicon surfaces was calculated at 42.8 mJ/m^2.

4. Results and discussion

Table 2 indicates how the surface roughness on the silicon samples changed during 100 cycles of testing. The mean RMS roughness Rq and the mean RMS peak asperity height σ_s are given for samples scanned both before and after testing. It is clear that a significant wear-induced

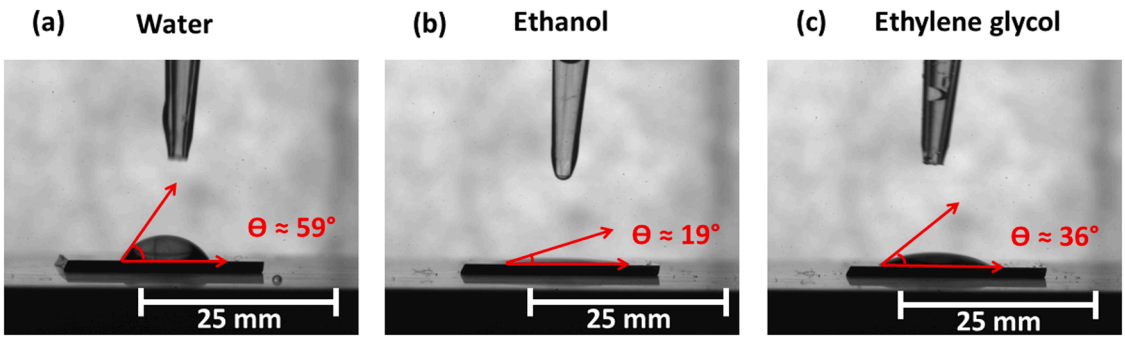

Fig. 3. Measurement of wetting contact angles for: (a) Water (b) Ethanol and (c) Ethylene glycol in contact with the silicon specimen surfaces for calculation of surface energy using the OWRK method [41].

Table 2
Average RMS roughness *Rq* and average RMS asperity peak height σ_s for silicon samples before and after 100 cycles of reciprocating sliding (bracketed values are standard deviations).

No. of samples	RMS Roughness *Rq* (nm)		RMS asperity peak height σ_s (nm)	
	Before	After	Before	After
1st	0.16 ± 0.004	28.9 ± 42.0	0.12 ± 0.003	26.9 ± 44.4
2nd	0.17 ± 0.07	35.8 ± 48.9	0.22 ± 0.20	35.4 ± 51.6
3rd	0.64 ± 0.44	29.1 ± 52.8	1.09 ± 0.9	27.2 ± 52.8
4th	0.32 ± 0.04	31.3 ± 47.1	0.47 ± 0.07	28.3 ± 48.1
5th	0.31 ± 0.27	27.8 ± 43.8	0.36 ± 0.30	22.01 ± 39.8

increase in surface roughness has occurred. On average (for the five repeat tests), Rq was 0.32 nm before testing, but had risen to 30.6 nm after 100 cycles of reciprocating sliding. Standard deviations are high for the post-test roughness values: this is because of wide variation in roughness levels across the worn surfaces i.e. from areas of worn tracks to more unworn areas etc.

The evolution of the tangential force (from stick to full slip) in the first 12 cycles of testing are shown in Fig. 4a. The measured roughness evolution during the tests was then used to predict the equivalent tangential force evolution using the Xu et al. model [14] (σ_s being the key model input) and the result (also for the first 12 cycles) is given in Fig. 4b. Note: only results from the forward stroke are shown here for comparison with the model – the reverse stroke is similar and the full hysteresis loops are given in the Appendix (Fig. A1). What the results show is that a prominent static friction peak is very much apparent in the initial cycles of reciprocating sliding, but that it largely disappears after relatively few cycles. In Fig. 4a, Cycle 1 has the most prominent peak and, by Cycle 12, the peak is vastly reduced. As the cycles of reciprocating sliding are nominally identical, this suggests that wear must be

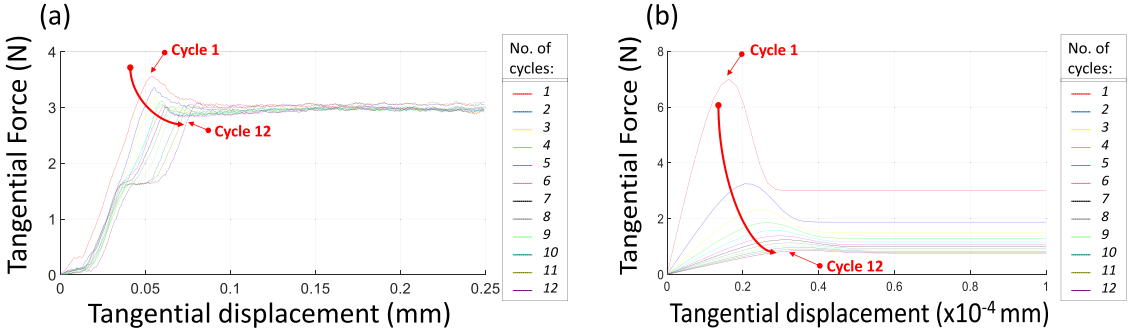

Fig. 4. Tangential force versus displacement plots indicating the evolution of the static friction peak in the first 12 cycles for (a) a representative reciprocating sliding experiment and (b) the prediction from the Xu et al. multi-asperity friction model based on an evolving surface roughness. Note, the experimental plot in (a) shows only part of the forward sliding stroke (up to 0.25 mm displacement). Full hysteresis loops for (a) are given in Fig. A1 in the Appendix.

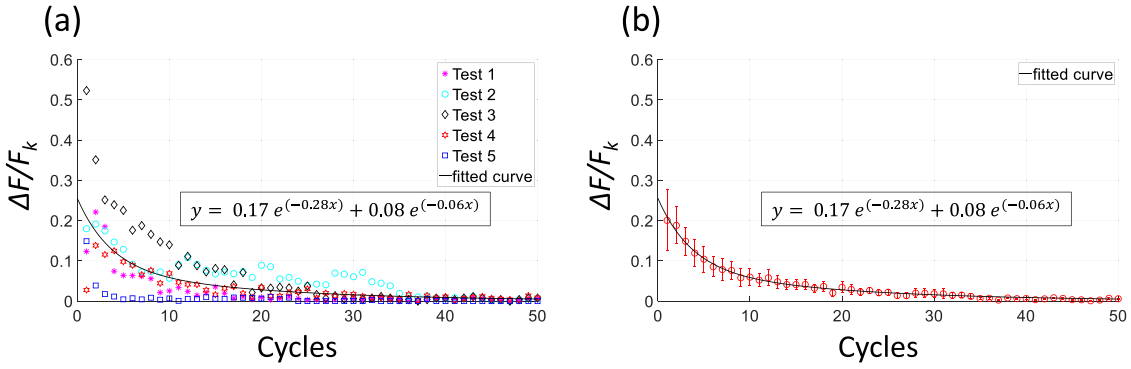

Fig. 5. Relative static friction peak ($\Delta F/F_k$) versus number of cycles from experiment showing: (a) individual results from each of the five tests and (b) the average result from the five tests. Note: the best fit exponential curve fit is also plotted.

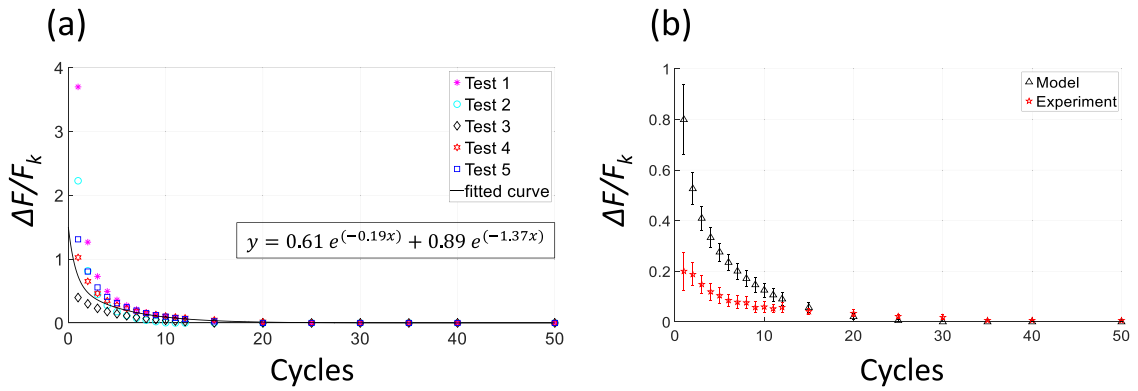

Fig. 6. (a) Relative static friction peak ($\Delta F/F_k$) versus number of cycles as predicted by the Xu et al. multi-asperity friction model [14] based on the roughness evolution estimated for each of the five experiments (including best fit exponential curve) and (b) Comparison of average results from the Xu et al. model [14] with experiment.

responsible for erasing the peak. In terms of the Xu et al. multi-asperity model [14], we account for this wear effect by inputting the cycle dependent surface roughness as estimated from surface scans. This produces the result shown in Fig. 4b. Although the predicted magnitudes of the friction forces are somewhat different (discussed later), the model also predicts a static friction peak decaying rapidly with number of cycles. The model helps offer one possible explanation for the wear induced decay in the static friction peak. Since increasing roughness for each cycle is the only variable input to the model, the model suggests that an increasing surface roughness due to wear can (potentially) explain the decay in the static fiction peak. It is worth noting that the kinetic friction level for Cycle 1 is in agreement in both model and experiment (both are about 3 N). Since kinetic friction is determined by $F = \tau A_r$, this indicates that, at least the product of τA_r is correct in Cycle 1 of the modelling result (it also indicates that the τ value chosen from the literature must be reasonably accurate). After the first cycle, the kinetic friction in the model (Fig. 4a) remains nearly constant up to 100 cycles of sliding. However, in the model, because τ is assumed constant (for silicon-on-silicon), the product of τA_r (i.e. the kinetic friction) reduces with number of cycles (see Fig. 4b). This is simply because of the reducing A_r (with No. of cycles) which arises in the model because of the increasing surface roughness. This perhaps suggests that the interfacial shear strength τ may not be constant during the test, but we are not in a position to assume this in the absence of direct measurements of interfacial shear strength. Note that, for some cycles, a rigid body shift of the interface occurred (at a tangential force of about 1.6 N – see Fig. 4a), but this has no bearing on the limiting friction (static or kinetic).

The relative static friction peak ($\Delta F/F_k$) for each of the five repeat tests is plotted against number of cycles of reciprocating sliding in Fig. 5a (up to 50 cycles) and the mean result is given in Fig. 5b. Fig. 6a shows the evolution of $\Delta F/F_k$ from the Xu et al. model [14] based on estimated roughness evolution in the five tests and Fig. 6b compares the mean experimental result with the mean result from the model. In the experiments, the static friction peak is (on average) about 25% of the kinetic friction level in the first cycle, but decays to a negligible level after only 30 cycles of sliding (Fig. 5b). The general form of the decay is exponential as indicated by the best fit exponential-based functions added in Fig. 5. The model predicts a similar trend (see Fig. 6), although the magnitudes of the relative peaks are somewhat different (Fig. 6b). This is because the magnitudes of static and kinetic friction differ between experiment and model. For kinetic friction, this is for the reasons already mentioned. For static friction, as we see in Fig. 4, the magnitudes differ between experiment (Fig. 4a) and model (Fig. 4b), but this is because the static friction in the model is calculated based on a complex multi-asperity implementation of asperity level fracture which is unlikely to find exact agreement with experiment in a macroscale contact partly due to errors introduced via the model in interface and material properties etc. In fact, the similarity in magnitudes is encouraging given the complexity and assumptions inherent in the model.

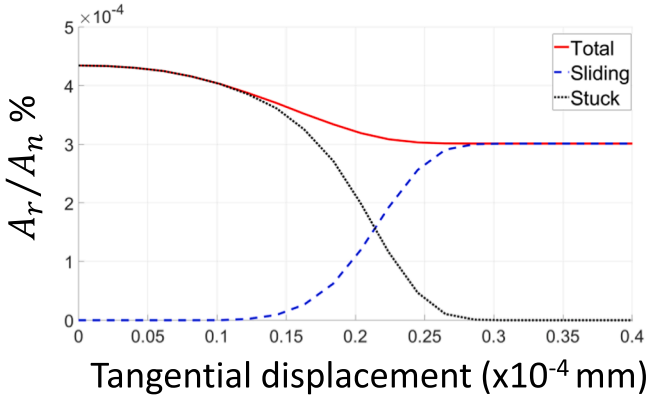

Fig. 7. Evolution of normalised real contact area percentage versus tangential displacement as predicted by the Xu et al. multi-asperity friction model [14] for Cycle 1 using the test surfaces corresponding to Fig. 4a. The plot illustrates how the contact area in the stick state and the sliding contact area evolve and combine to determine the evolution of the total A_r. The higher fully stuck contact area (at zero displacement) as compared to the contact area in sliding (beyond about 0.3×10^{-4} mm displacement) is one of the key factors producing the static friction peak predicted by the model (see Fig. 4b).

We turn now to exploring exactly why the model predicts a static friction peak and to exactly how increasing surface roughness (with cycles) might lead to a decaying peak. Fig. 7 shows how the real contact area (normalised by A_n) evolves during the transition from 'fully stuck' to 'full sliding' when the Xu et al. model [14] is applied to Cycle 1 of one of the experimental interface pairs. The 'total' real contact area (at any value of tangential displacement) is the sum of the stuck contact area and the 'sliding' contact area. One of the contributors to the friction force peak (in the model) is the fact that, when a force peak is observed, the fully stuck contact area (i.e. at zero tangential displacement) is usually greater than the sliding contact area (i.e. beyond 0.3×10^{-4} mm in Fig. 7). The other reason is that, the static friction force in the model is determined by fracture of the stuck asperity junctions; whereas, the kinetic friction is governed by $F_k = \tau A_r$. So, factors such as high interfacial work of adhesion and low mode mixity (and indeed low values of τ) also contribute to the situation when $F_s > F_k$. In the experiments, the static friction force F_s reduces with number of cycles while the kinetic friction remains roughly constant (Fig. 4a). This can be explained by referring to Fig. 8 which plots the modelled evolution of the fully stuck real contact area with number of cycles in Fig. 8a and the corresponding evolution of F_s in Fig. 8b. The argument based on roughness is as follows.

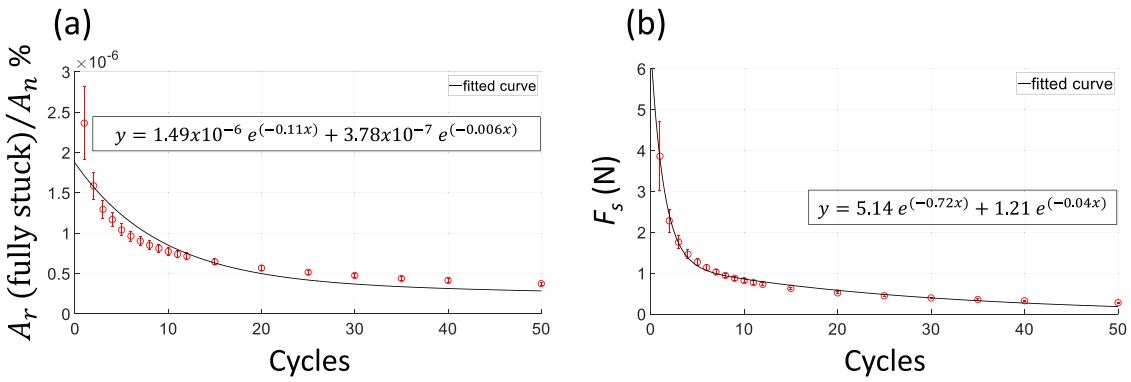

Fig. 8. (a) Mean fully stuck real contact area (at zero displacement) as a percentage of nominal contact area versus number of cycles as predicted by the Xu et al. model [14] (based on the measured roughness evolution in each test) and (b) Static friction force F_s versus number of cycles from the Xu et al. [14] model.

Surface roughness increases with cycles due to wear (see Table 2). This causes the fully stuck real contact area to reduce with cycles (Fig. 8a) and this results in the reduction in F_s with cycles (Fig. 8b).

The argument based on evolving roughness is only one possible explanation. We have considered it in detail above because of the considerable increases in roughness detected and because the Xu et al. model permits an explanation based on roughness. However, there are other scenarios which need to be considered. Another possibility is that repeated cycles of wear reduce the strength of the fully stuck interface. In the Xu et al. model [14], this could be accounted for via a reducing interfacial work of adhesion with cycles. Similarly to what we have shown for increasing roughness, this scenario would produce a friction force peak decay similar to that in Fig. 4b (and Fig. 6a) – see Xu et al. [14] for more details on the effect of work of adhesion. In this regard, a possible mechanism is that, thin layers of third body molecules that act to initially lock the surfaces together, get rubbed off after a few cycles of reciprocating sliding. For example, He et al. [18] mentioned that small hydrocarbon molecules adsorb on any surface exposed to air and can arrange to lock two contacting surfaces together. Li et al. [7] called attention to the possible mechanism of hydrogen bonding in the presence of contaminant molecules such as H_2O. If these are the dominant reason for the static friction peak at the beginning of reciprocating sliding, then it is reasonable that a few cycles of sliding could wear away the responsible molecular layers. With a hard brittle single-crystal material like Silicon, it is unlikely that creep induced contact area growth could be responsible for the initial peak in Cycle 1. In this case, and given that the initial roughness is very low ($Rq \approx 0.32$ nm), it appears that the chemical bonding argument is more realistic. An interesting aspect that arises in the reciprocating sliding test is that, the first cycle occurs after a dwell time (3 min in these experiments), but the stuck time is very small for subsequent cycles as the contact reverses direction and resumes sliding in a matter of milliseconds at the end of each stroke. What is interesting here is that several of the subsequent cycles (Cycle 2 to at least Cycle 12) also produce a distinct static friction peak (albeit decaying). There is certainly not enough time available during the motion reversal for creep induced contact area growth of the fully stuck contact. However, chemical bonding processes can be rapid and we can assume that there is sufficient time to reform bonds here during motion reversal. Finally, it is possible that both wear induced roughness changes and wear induced removal of surface layers contribute simultaneously to the observed wear-induced static friction peak decay observed here in reciprocating sliding. Finally, it is worth returning to the question of why the static friction peak is mostly absent in gross-slip fretting tests in the literature. The absence of the peak is probably because the data reported in results are generally from cycles occurring long after the test initiated meaning that enough cycles have already occurred to produce both wear-induced removal of initial surface layers and wear-induced increases in roughness. Also, most of the fretting test data comes from metal-to-metal contact and not enough time will be available during motion reversal (at the end of each reciprocating sliding stroke) for the kind of creep induced aging that can occur with static metal contacts.

5. Conclusions

This paper has set out to investigate why the static friction peak is very often absent in literature on reciprocating sliding and gross-slip fretting. Using reciprocating sliding tests on ultra-smooth samples cut from flat Silicon wafers ($Rq \approx 0.32$ nm), we find that a prominent static friction peak is present in the initial cycles of reciprocating sliding, but that it decays relatively quickly and has mostly disappeared by about 30 cycles. Therefore, the reason the peak is often absent may be because hysteresis loops are often reported for cycles well after the initial cycles (due to running-in periods etc.). As the sliding cycles are nominally identical, we attribute the decaying static friction peak to wear processes. In the experiments, the reduction in the friction peak took the form of static friction reducing with cycles with the kinetic friction level remaining roughly constant. Results also showed that surface roughness increased significantly with cycles of testing. Two main explanations are advanced for the wear-induced decay. The first is that significant increases in roughness during the test lead to reduction in the fully stuck real contact area (with cycles); thereby, producing a corresponding reduction in the static friction force. Applying the Xu et al. multi-asperity friction model [14] to the test surfaces, we showed that implementing the measured roughness reduction in the model predicts a similar static friction peak decay. The second possibility is that the initial static friction peak is caused by bonding involving third body contaminant molecules such as hydrocarbons or water and that subsequent cycles of sliding removes these layers leading to a somewhat weaker fully stuck interface in later cycles. Weakening of the fully stuck interface (with initial cycles) can also generate static friction peak decay in the Xu et al. model (via reduced work of adhesion). As Silicon is a brittle single crystal material, creep induced growth of the contact area is an unlikely explanation for the static friction peak here. This is also confirmed by the appearance of the peak in cycles following the first cycle where time available for junction growth (of the real contact area) is insufficient as the reciprocating contact reverses direction in milliseconds. Therefore, a stronger chemical bond in the fully stuck case is the most likely explanation. It may be that both surface roughness changes and molecular layer removal both contribute to the behaviour. However, the exact origin of the wear-induced decay observed here in reciprocating sliding requires more investigation.

Declaration of Competing Interest

The authors declare that they have no known competing financial interests or personal relationships that could have appeared to influence

the work reported in this paper.

Data Availability

Data will be made available on request.

Acknowledgments

The authors would like to acknowledge the support of the Leverhulme Trust who supported the overall research under project grant "Fundamental Mechanical Behaviour of Nano and Micro Structured Interfaces" (RPG-2017-353). S.B-J acknowledges the support of the Saudi Arabian Cultural Bureau in London and Al-Imam Mohammad Ibn Saud Islamic University (IMISU), Riyadh for sponsoring and supporting his Ph.D. studies. N.G. acknowledges ERC funding through FAKIR 648892 Consolidator Award and support from the Research Council of Norway through its Centres of Excellence funding scheme, Project No. 262613. Staff at Glasgow's James Watt Nanofabrication Centre (JWNC) are thanked for their support. Dr Jacek Olender (University of Glasgow) is thanked for his advice on surface energy measurement.

Appendix

Fig. A1.

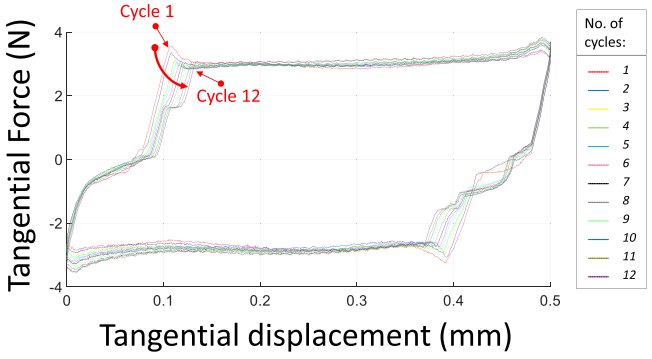

Fig. A1. Representative full reciprocating sliding hysteresis loops corresponding to Fig. 4a showing tangential force versus tangential displacement for the first 12 cycles of testing (Stroke length = 0.5 mm).

References

[1] Rabinowicz E. The nature of the static and kinetic coefficients of friction. J Appl Phys 1951;vol. 22(11):1373–9.
[2] Persson BNJ, Albohr O, Mancosu F, Peveri V, Samoilov VN, Sivebaek IM. On the nature of the static friction, kinetic friction and creep. Wear 2003;vol. 254(9):835–51.
[3] Baumberger T, Berthoud P, Caroli C. "Physical analysis of the state- and rate-dependent friction law. II, Dynamic friction. *Phys Rev B* 1999;vol. 60(6):3928–39.
[4] Gitis NV, Volpe L. Nature of static friction time dependence. J Phys D: Appl Phys 1992;vol. 25(4):605–12.
[5] Dieterich JH. Modeling of rock friction: 1. Experimental results and constitutive equations. J Geophys Res: Solid Earth 1979;vol. 84(B5):2161–8.
[6] Li S, Zhang S, Chen Z, Feng X-Q, Li Q. Length scale effect in frictional aging of silica contacts. Phys Rev Lett 2020;vol. 125(21):215502.
[7] Li Q, Tullis TE, Goldsby D, Carpick RW. Frictional ageing from interfacial bonding and the origins of rate and state friction. Nature 2011;vol. 480(7376):233–6.
[8] Lorenz B, Persson BNJ. On the origin of why static or breakloose friction is larger than kinetic friction, and how to reduce it: the role of aging, elasticity and sequential interfacial slip. J Phys: Condens Matter 2012;vol. 24(22):225008.
[9] Bowden FP, Tabor D. The friction and lubrication of solids. Oxford: Clarendon Press; 1950.
[10] Weber B, Suhina T, Brouwer AM, Bonn D. Frictional weakening of slip interfaces. Sci Adv 2019;vol. 5(4):eaav7603.
[11] Sahli R, et al. Evolution of real contact area under shear and the value of static friction of soft materials. Proc Natl Acad Sci USA 2018;vol. 115(3):471–6.
[12] Budakian R, Putterman SJ. Time scales for cold welding and the origins of stick-slip friction. Phys Rev B 2002;vol. 65(23):235429.
[13] Filippov AE, Klafter J, Urbakh M. Friction through dynamical formation and rupture of molecular bonds. Phys Rev Lett 2004;vol. 92(13):135503.
[14] Xu Y, Scheibert J, Gadegaard N, Mulvihill DM. An asperity-based statistical model for the adhesive friction of elastic nominally flat rough contact interfaces. J Mech Phys Solids 2022;vol. 164:104878.
[15] Papangelo A, Ciavarella M. On mixed-mode fracture mechanics models for contact area reduction under shear load in soft materials. J Mech Phys Solids 2019;vol. 124:159–71.
[16] J.A. Greenwood and J.B.P. Williamson, "Contact of nominally flat surfaces," Proceedings of the Royal Society of London. Series A, Mathematical and Physical Sciences, vol. 295, no. 1442, pp. 300–319, 1966.
[17] Vlassov S, et al. Complex tribomechanical characterization of ZnO nanowires: nanomanipulations supported by FEM simulations. Nanotechnology 2016;vol. 27(33):335701.
[18] He G, Müser MH, Robbins MO. Adsorbed layers and the origin of static friction. Science 1999;vol. 284(5420):1650–2.
[19] Tabor D, Bowden FP. Junction growth in metallic friction: the role of combined stresses and surface contamination. Proc R Soc Lond Ser A Math Phys Sci 1959;vol. 251(1266):378–93.
[20] Bowden FP, Young JE. Friction of clean metals and the influence of adsorbed films. Proc R Soc Lond Ser A Math Phys Sci 1951;vol. 208(1094):311–25.
[21] Ovcharenko A, Halperin G, Etsion I, Varenberg M. A novel test rig for in situ and real time optical measurement of the contact area evolution during pre-sliding of a spherical contact. Tribol Lett 2006;vol. 23(1):55–63.
[22] Etsion I. Revisiting the Cattaneo–Mindlin concept of interfacial slip in tangentially loaded compliant bodies. J Tribol 2010;vol. 132(2).
[23] Mulvihill DM, Kartal ME, Olver AV, Nowell D, Hills DA. Investigation of non-Coulomb friction behaviour in reciprocating sliding. Wear 2011;vol. 271(5–6):802–16.
[24] Kartal ME, Mulvihill DM, Nowell D, Hills DA. Measurements of pressure and area dependent tangential contact stiffness between rough surfaces using digital image correlation. Tribol Int 2011;vol. 44(10):1188–98.
[25] Kartal ME, Mulvihill DM, Nowell D, Hills DA. Determination of the frictional properties of titanium and nickel alloys using the digital image correlation method. Exp Mech 2011;vol. 51(3):359–71.
[26] Fantetti A, et al. The impact of fretting wear on structural dynamics: experiment and simulation. Tribol Int 2019;vol. 138:111–24.
[27] Fouvry S, Liskiewicz T, Kapsa P, Hannel S, Sauger E. An energy description of wear mechanisms and its applications to oscillating sliding contacts. Wear 2003;vol. 255(1–6):287–98.
[28] Magaziner R, Jin O, Mall S. Slip regime explanation of observed size effects in fretting. Wear 2004;vol. 257(1–2):190–7.
[29] Magaziner RS, Jain VK, Mall S. Wear characterization of Ti-6Al-4V under fretting-reciprocating sliding conditions. Wear 2008;vol. 264(11–12):1002–14.
[30] Everitt NM, Ding J, Bandak G, Shipway PH, Leen SB, Williams EJ. Characterisation of fretting-induced wear debris for Ti-6Al-4V. Wear 2009;vol. 267(1–4):283–91.
[31] Eriten M, Polycarpou A, Bergman L. Development of a lap joint fretting apparatus. Exp Mech 2011;vol. 51(8):1405–19.
[32] Hintikka J, Lehtovaara A, Mäntylä A. Non-Coulomb friction in gross sliding fretting conditions with aluminium bronze against quenched and tempered steel. Tribol Int 2014;vol. 79:151–61.
[33] Hintikka J, Lehtovaara A, Mäntylä A. Fretting-induced friction and wear in large flat-on-flat contact with quenched and tempered steel. Tribol Int 2015;vol. 92:191–202.
[34] Hintikka J, Mäntylä A, Vaara J, Frondelius T, Juoksukangas J, Lehtovaara A. Running-in in fretting, transition from near-stable friction regime to gross sliding. Tribol Int 2020;vol. 143:106073.
[35] Hintikka J, Lehtovaara A, Mäntylä A. Normal displacements in non-Coulomb friction conditions during fretting. Tribol Int 2016;vol. 94:633–9.
[36] Jaber SB, Hamilton A, Xu Y, Kartal ME, Gadegaard N, Mulvihill DM. Friction of flat and micropatterned interfaces with nanoscale roughness. Tribol Int 2021;vol. 153:106563.
[37] ASTM D1894–14, Standard Test Method for Static and Kinetic Coefficients of Friction of Plastic Film and Sheeting, ASTM International, West Conshohocken, PA, 2014.
[38] Sayles RS, Thomas TR. Measurements of the statistical microgeometry of engineering surfaces. J Lubr Technol 1979;vol. 101(4):409–17.
[39] Wortman JJ, Evans RA. Young's modulus, shear modulus, and Poisson's ratio in silicon and germanium. J Appl Phys 1965;vol. 36(1):153–6.
[40] Umeno Y, Kitamura T. Ab initio simulation on ideal shear strength of silicon. Mater Sci Eng: B 2002;vol. 88(1):79–84.
[41] Owens DK, Wendt RC. Estimation of the surface free energy of polymers. J Appl Polym Sci 1969;vol. 13(8):1741–7. https://doi.org/10.1002/app.1969.070130815.
[42] Schuster JM, Schvezov CE, Rosenberger MR. Analysis of the results of surface free energy measurement of Ti6Al4V by different methods. Procedia Mater Sci 2015;vol. 8:732–41.
[43] Tokuda M, Shindo T, Minami H. Preparation of polymer/poly(ionic liquid) composite particles by seeded dispersion polymerization. Langmuir 2013;vol. 29(36):11284–9.